

Preparation and Characterization of Tungsten Oxide Thick Film Gas Sensor

K. B. Bhamare¹, T. R. Mahale² And R. Y. Borse³

¹(Department of Physics, L.V. H. College, Panchwati, Nasik-3, India)

²(Department of Chemistry, L.V. H. College, Panchwati, Nasik-3, India)

³(Department of Physics, M. J. M. College, Karanjali (Peth) Nasik, India)

Corresponding Author: K. B. Bhamre

Abstract: Tungsten oxide (WO_3) thick films are prepared by screen printing method for detection of pollutant gases. WO_3 thick films characteristics was investigated for X-ray diffraction to determine the structure and phases. The X-ray diffraction patterns indicate that the thick films fired at 600, 700 and 800°C are polycrystalline. Surface morphological and compositional characterizations of the prepared pure WO_3 thick films were determined using SEM with EDAX. The temperature dependent electrical resistance variations for pure WO_3 thick films were investigated. The electrical resistivity, TCR, activation energy of pure WO_3 thick films was obtained. WO_3 thick film Sensor response is investigated for various gases for different concentrations. It is found that tungsten oxide based thick film sensor is a good candidate for NO_2 sensors with satisfactory response and recovery times. The sensing mechanism associated with NO_2 gas detection is also discussed. The prepared sensor is characterized by XRD and SEM.,

Keywords - Tungsten trioxide, thick film sensor, resistivity, TCR, SEM and XRD, sensitivity

Date of Submission: 21-06-2018

Date of acceptance: 09-07-2018

I. Introduction

Tungsten trioxide is inorganic chemical compound containing oxygen and the transition metal tungsten. It is obtained as an intermediate in the recovery of tungsten from its minerals. Tungsten ores are treated with alkalis to produce WO_3 . It possesses a polycrystalline structure. Semiconducting metal oxides has proved to be very prominent member for detecting and monitoring the emission of pollutant gases. Their sensing principle is based on the change in the resistance of a semiconductor metal oxide film when specific gases interact with its surface. The surface of the semiconductor provides different surface states and when gas molecules are adsorbed and react at the semiconductor surface a change in the inter-grain barrier height occurs. So, the basic principle of operation of a semiconductor gas sensor is the control of surface potential barrier by adsorbent. Tungsten oxide films are n-type semiconductors with a band gap of 2.6-2.8eV [1, 2] having a strong absorption within the solar spectrum (440 nm) that exhibit superior electronic and optical properties. Tungsten has many oxidation states i.e. 2,3,4,5 and 6 [3]. In recent years; WO_3 has been studied for its gas sensing properties, making it about the fifth most researched metal oxide for this purpose [4]. Tungsten also forms other oxides such as WO , W_2O_3 and W_4O_{11} , however in gas sensing the stable WO_3 form is used. The crystal structure of tungsten trioxide is temperature dependent, shows five phase transitions with the sequence viz. tetragonal at temperatures above 740 °C, orthorhombic from 330 to 740 °C, monoclinic from 17 to 330 °C, and triclinic from -50 to 17 °C. Many researchers pointed out that these phases are affected by many factors including temperature, impurity and substrate material. These films have been widely studied for various applications such as photo catalysis [5], high density memory devices, smart windows [6], gas sensor [7, 8], photoelectrochemical water splitting, and electrochromism [9-11].

Electrical and optical characteristics of tungsten trioxide are dependent on the crystalline structure [12-16]. In addition to the above phases, a metastable hexagonal WO_3 phase has also been reported around 400°C [17]. Gullapalli et al. have successfully deposited tungsten trioxide thin films by using radio frequency reactive magnetron Sputtering technique [18] and conclude that the films prepared at 100-300 °C could be the best

candidate for H₂S gas sensor applicable in coal gasification system. Sulfur is highly toxic and it is a natural contaminant in fossil fuel supplied. They aware that the amount of H₂S produced from coal gasification Plant must be effectively controlled and monitored. Nishchay et al. [19] prepared tungsten oxide films using spark ablation and focused inertial deposition technique. They produced various crystal structured materials by controlling the experimental conditions. They pointed out that, the as-deposited films and annealed films (at 500°C) are amorphous and crystallite, respectively. Lastly, they conclude that the obtained films provide high sensitivity and high accuracy in application for NO₂ gas sensing. Wongchoosuk et. al. have been studied Multi-walled carbon nanotube-doped tungsten oxide thin films for hydrogen gas sensing application [20].

In the present work, thick films of tungsten trioxide have been deposited on alumina substrate by using screen printing method and the general properties such as structural, elemental analysis, surface morphology and band gap of thick films can be investigated. The obtained thick films are characterized for gas sensing will be discussed and different gas sensing parameters are evaluated.

II. Methods

2.1. Powder, Paste and Thick Film Preparation

Commercially available lemon yellow colour WO₃ powder (Sigma Aldrich) is mixed thoroughly in an acetone medium by using a mortar and pestle with a permanent binder as a glass frit [21, 22]. Initially the fine powder is calcined at 450 °C for 2 hours in muffle furnace. The pastes used for screen- printing were prepared by maintaining inorganic to organic materials ratio of 70:30. The inorganic part consisted of a functional material (WO₃) and glass frit. The organic part consisted of ethyl cellulose (EC) as temporary binder and butyl carbitol acetate (BCA) as solvent. The mixture of WO₃ powder, glass frit and ethyl cellulose was mixed thoroughly by adding butyl carbitol acetate drop by drop until a proper thixotropic property of paste was achieved. Then the paste was screen printed onto an alumina substrate (96% pure) to prepare thick film resistor [22-29]. The films were then dried under IR lamp for 1 hour in an air to remove the temporary organic binder and fired at 600, 700 and 800 °C for 2 hours in the muffle furnace for better adhesion. During the firing process glass frit melts and the functional materials are sintered. The function of glass frit is to bind grains of functional material together. The thickness of the WO₃ thick films resistors were measured by using gravimetric method. The thickness of the films was observed in the range of 10µm to 25µm.

2.2. Structural and Morphological Characterization

In order to understand the structural phases, X-ray diffraction [Mini Flex model Rigaku 2500, Japan] was carried out in the range of 20-80°, (2θ) using CuKα radiation. The average grain sizes of tungsten oxide thick film samples were calculated by using the Scherer formula [30]:

$$D = \frac{0.9\lambda}{\beta \cos\theta} \quad (1)$$

where D = the average grain size,
λ = 1.542 Å (X-ray wavelength), and
β = the peak FWHM in radiation and
θ = diffraction peak position.

The microstructure and chemical composition of the films were analyzed using a scanning electron microscope [SEM-JOEL JED 2300] coupled with an energy dispersive spectrometer [6360 LA].

The average particle size was measured from SEM and specific surface area was calculated for spherical particles using the following equation [31, 32].

$$S_w = \frac{6}{\rho d} \quad (2)$$

where d is the diameter of the particles, ρ is the composite density of the particles.

2.3. Electrical properties and Gas sensing response

The resistance of the WO₃ thick films was measured by using half bridge method at different temperature [21, 22, 33, 34]. Sheet resistance (ρ_s) defined as resistivity per unit thickness (t) of the WO₃ thick film was calculated by the equation.

$$\text{Sheet resistance} = \rho_s = \frac{\rho}{t} = \frac{R \times b}{l} \quad (3)$$

Where b = breadth of WO_3 thick film resistor sensors in meters,
 l = length of WO_3 thick film resistor sensors in meters.

The effect of temperature on the resistance of the WO_3 thick film resistor sensors was studied to determine the Temperature Coefficient of Resistor (TCR) and calculated as

$$\text{TCR} = \frac{1}{R_o} \left(\frac{\Delta R}{\Delta T} \right) \times 10^6 \text{ ppm/}^\circ \text{K} \quad (4)$$

Where ΔR = change in resistance from temperature range T_1 to T_2 ,
 ΔT = temperature difference between T_1 and T_2 ,
 R_o = Initial resistance of the film sample.

The activation energy of WO_3 thick films was calculated by the Arrhenius plot using the relation,

$$R = R_o e^{-\Delta E/KT} \quad (5)$$

Where R_o = constant,
 ΔE = the activation energy of the electron transport in the conduction band,
 K = Boltzmann constant and
 T = Absolute temperature.

2.4. Gas sensing set up

The gas sensing measurements of the WO_3 thick film sensor were tested on indigenously developed static gas characterization system. The test system consisted of a glass chamber of diameter 10 cm and 15 cm height. Effective volume of the chamber was 2000ml. An inlet was provided for inserting desired concentration of gas to the chamber. An outlet is also provided to remove the gas. The pre-calibrated gas cylinders were obtained from laboratories. The gas was injected into test chamber with a syringe through an inlet provided with septum. Electrical connections from the sensor were made using two thin copper wires, bonded to the sensor with silver paint. The sensing capability of the sensor was characterized at different operating temperatures to find out optimum working temperature. A heater is incorporated in the chamber in order to heat sample to desired temperature. A chrome-Alumel thermocouple is used to sense temperature. Feedthroughs are provided at the bottom of the chamber for electrical connections to the heater as well as for the temperature sensor. Electrical characterization of the WO_3 thick films with and without gas was obtained by measuring the change in resistance of films. A digital multimeter is used to measure the resistance of the sensor.

The gas sensing studies of WO_3 thick films fired at 600°C were carried out for different gases at 500 ppm in a static gas sensing system [21, 22, 35, 36] under normal laboratory conditions. The gas sensitivity, S_{ra} of the WO_3 thick film sensor is calculated by using the relation,

$$S_{ra} = \frac{R_{air} - R_{gas}}{R_{air}} \quad (6)$$

Where R_a is the resistances of the thick film resistors in air and

R_g is the resistances of the WO_3 thick film resistors in gas atmosphere.

III. Results and Discussion

3.1. X-ray diffraction analysis of WO_3 thick films

In the present paper we prepared WO_3 thick film resistor as a gas sensors using standard screen printing method. To understand the structural phases of WO_3 thick films fired at 600, 700, and 800°C , XRD was employed. The surface morphology, phase composition and specific surface area were analyzed by SEM and EDAX. The XRD pattern shows several peaks of WO_3 phases confirming polycrystalline nature. In Fig. 1, the peak intensity of WO_3 thick film resistors, which is a characteristic of crystallization, rises with increasing firing temperatures. This means that the crystallinity is enhanced at higher firing temperature. By comparing the data we obtained with those of PDF (Powder Diffraction file) number 20-1324 and 43-1035, we concluded that the experimental data were agreed with a monoclinic and some orthorhombic phases of WO_3 .

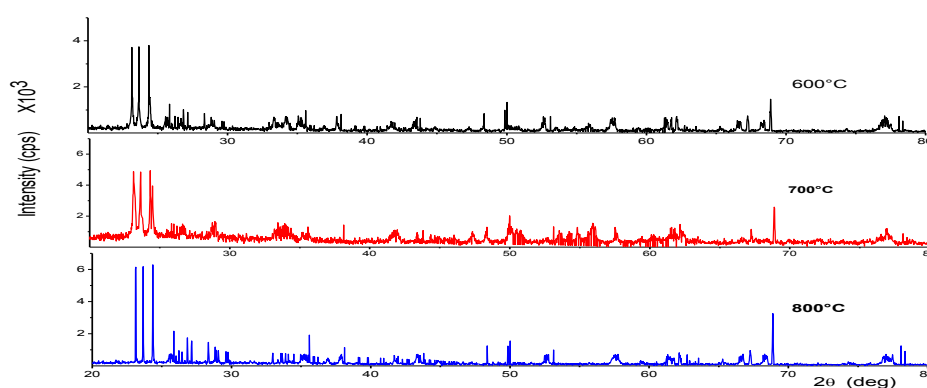


Fig.1 X-Ray diffraction pattern of WO_3 thick films fired at (a) 600 (b) 700 and (c) 800°C

Major peaks were found at $2\theta = 23.12, 23.62$ and 24.32° , which were identified as corresponding to Miller index (002), (200) and (020) respectively, in monoclinic and some orthorhombic structure of WO_3 (O-20-1324;M-43-1035) and other minor peaks in various directions. Therefore the thick film resistors of pure WO_3 obtained after firing at 600, 700 and 800°C was polycrystalline in nature. The other peaks at $58^\circ, 77.40^\circ$ correspond to the alumina substrate.

The crystallite size (D) was calculated from peaks using the Debye Scherer formula. The average crystallite size (D) of the pure WO_3 , thick film resistors fired at 600, 700 and 800°C were found to be 52.03nm, 55.86nm, and 59.90nm respectively. Crystallite size was estimated individually from the FWHM of each plane and the average of all the planes was taken to obtain the average crystallite size. Hence the thick film resistor sensors were identified by XRD as nanocrystalline in nature.

The sharp peaks reflexes seen on the pattern indicate that a transformation to a highly ordered crystallite has occurred in the material. From XRD analysis all films were shown random orientation of polycrystalline nature. It has been observed that (200) reflections at $2\theta = 24.32^\circ$ are of maximum intensity, which indicates that WO_3 films have preferred orientation in the (200) plane. The higher peak intensities of an XRD pattern is due to the better crystallinity and bigger grain size can be attributed to the agglomeration of particles. It is observed that as the firing temperature increases, the peak height also increases as shown in **Fig.1**. Hence the 600 °C fired nanocrystalline WO_3 thick film resistors were identified by XRD for best gas sensing characterizations.

3.2. Scanning Electron Microscopic analysis of WO_3 thick films

The information about the surface morphology, crystalline shape and size of thick film materials is obtained by using Scanning Electron micrographs (SEM) [SEM-JEOL, model- 6300(LA), Germany]. **Fig.2** shows SEM images of WO_3 thick films fired at 600, 700 and 800°C for studying the effect of firing temperature on surface morphology. These SEM images show that the particle size of the WO_3 thick film increases with rising firing temperature. All the SEM images are recorded at 100000X magnification for comparison. The SEM images show the distribution of particles and agglomerates to be affected with the firing temperature. It is evident that the material consists primarily of crystalline aggregates and is highly porous in nature. The most important factors that influence the films characteristics are probably microstructure and surface area. The films exhibiting a porous structure have a large fraction of atoms residing at surfaces and interfaces between the pores, which suggests that the microstructure of the films is suitable for gas-sensing purposes. The SEM images of WO_3 thick films shows polycrystalline structure with less or more numbers of pores (voids) on the surface of the films, basically due to evaporation of organic binder during the firing of the films. The particle size distribution of the resulting films was affected by the firing temperature. WO_3 thick films showed polycrystalline grain morphology consisting of spherical grains of grain size ranging from 93- 274 nm for firing temperature ranging from 600-800 °C. The average particle sizes of these WO_3 thick films is about 93.354, 174.19 and 273.8 nm (± 2 nm) for 600, 700 and 800°C respectively. However, large polycrystalline grains were formed by the necking or merging of small grains during the firing process. The average particle size observed in SEM is much higher than estimated from XRD data, indicating agglomeration of the particles.

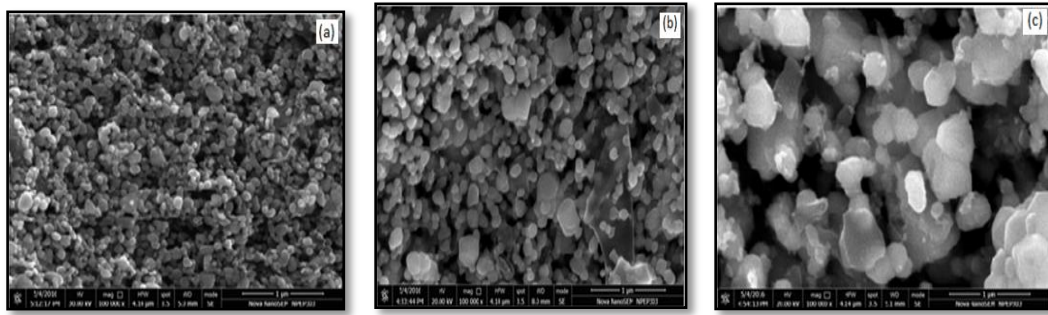


Fig. 2 SEM of pure WO₃ Thick Films fired at (a) 600°C, (b) 700°C and (c) 800°C

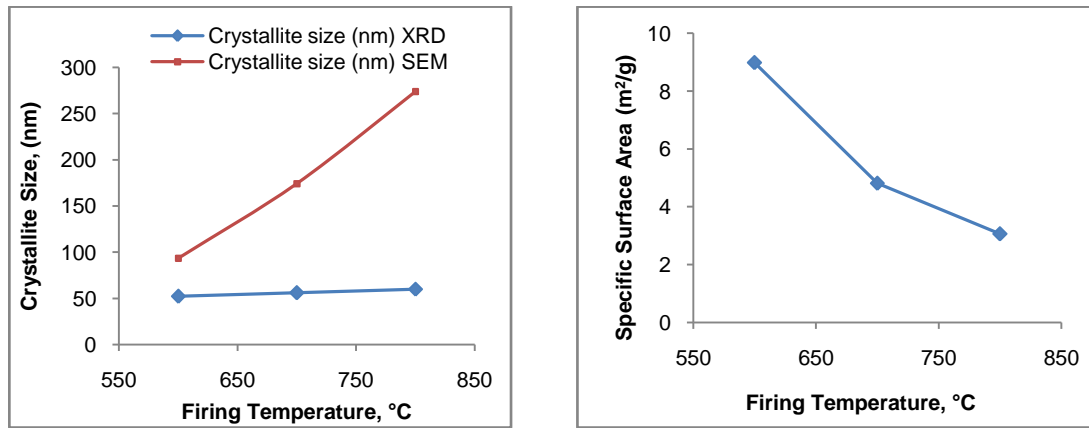


Fig.3 Plot of (a) particle size and (b) Specific surface area (S_w) versus firing temperature

The corresponding particle size data from SEM is plotted in Fig. 3(a) along with XRD data. Fig. 2 shows that particle size is increased with increase of firing temperature of WO₃ thick films. Fig. 3(b) shows the plot of Specific surface area versus firing temperature of WO₃ thick films indicating that Specific surface area is decreased with increase of firing temperature of the films.

3.3. EDAX Spectra of WO₃ thick films (Elemental analysis)

The EDAX analysis of WO₃ thick films fired at 600, 700 and 800°C was carried out using EDAX (JEON, JED-2300, Germany). Fig. 4 represents EDAX spectra of WO₃ thick film samples fired at different temperatures. The EDAX data indicate the appearance of peaks of the component in each WO₃ thick film material. The EDAX analysis showed presence of only W and O elements as expected, no other impurity elements were present in the film samples. The EDAX results show lot of variation in W/O ratio with firing temperature. It is found that high value of W/O ratio for WO₃ film is at 800°C firing temperature. Also from the EDAX spectra, it is found that wt% and At. wt. % of W and O is nearly matched as illustrated in Table-1.

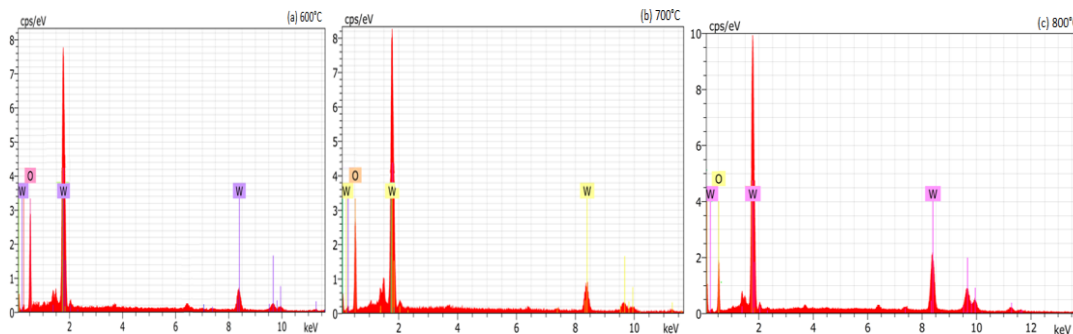


Fig. 4 EDAX Spectra of WO₃ thick films fired at (a) 600 (b) 700 and (c) 800°C

Table 1: Elemental composition

Firing temperature	Element	At. Wt. %	W/O ratio	Mass %	W/O ratio
600 °C	W	66.19	1.9577	95.74	22.4741
	O	33.81		4.26	
700 °C	W	69.47	2.2754	96.32	26.1739
	O	30.53		3.68	
800 °C	W	72.12	2.5868	96.74	29.6748
	O	27.88		3.26	

IV. Electrical and gas sensing characterization

4.1 Resistance-Temperature Relations

According to semiconductor theory, the relationship between semiconductor’s resistance and temperature can be approximated by a nonlinear function. The resistance as a function of temperature can be described as: $R_T = R_0 e^{-\Delta E/KT}$, where R_T and R_0 are the resistance values at absolute temperatures T and T_0 (on the Kelvin scale), respectively. ΔE is activation energy and K is Boltzmann constant over a limited temperature range. From this relationship, one can make conclusion that SMO thick films resistance is greatly affected by temperature. **Fig. 5** shows this relationship when thick film temperature changes from room temperature to 450°C, the thick film resistance decreases from higher to below minimum values.

The Electrical DC resistance of the tungsten oxide thick films fired at 600, 700 and 800°C ($\pm 5^\circ\text{C}$), were measured by half bridge method at different temperatures. The resistance of thick films decreases with increasing temperature indicating semiconducting behaviour. **Fig. 5(a)** shows the resistance variation of WO_3 thick films with temperature in air.

WO_3 thick films exhibited nearly three regions for change in resistance with temperature viz.: (i) continuous initial fall of resistance region, (ii) an exponential fall of resistance region and (iii) finally saturation region. Any increase in temperature of thick film causes the electrons to acquire enough energy and cross the barrier at grain boundaries [21, 37]. There may be decrease in potential barrier at grain boundaries, since at higher temperature the oxygen adsorbents are desorbed from the surface of the films. There is a decrease in resistance with increase in temperature indicating semiconducting behaviour, obeying $R = R_0 e^{-\Delta E/KT}$ in the temperature range of 30 to 450 °C. For WO_3 thick films fired at 600-800 °C, initially resistance is falls linearly up to a certain transition temperature. After that transition temperature the resistance decreases in exponential type and finally saturates to steady level. The transition temperature depends on firing temperature of the thick film. The initially value of WO_3 thick film resistance in air atmosphere at 30 °C was 9667, 6882, 2742 MΩ fired at 600, 700, 800 °C respectively may be due to change in thickness.

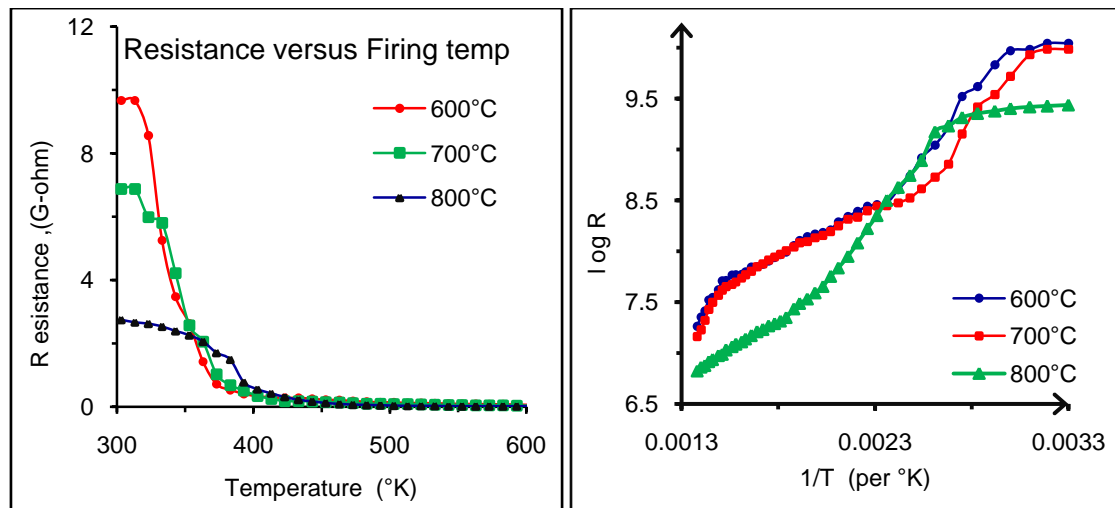


Figure 5: Variation of (a) Resistance with temperature and (b) log R Vs 1/T of WO_3 thick film fired at 600,700 and 800 °C.

The experimental results have been interpreted in terms of various conduction mechanisms such as thermionic emission, Schottky emission, tunneling allowed states. According to Nifontoff [38] the thermionic emission and Schottky emission predominates only when the separation of particles is more than 100 \AA . The electrical properties of thick films are functions of many factors such as manufacturing technique, ingredients and sintering history [39]. The main ingredient of thick film is a conducting phase, such as oxides; a dielectric phase, such as glass frit; and an insulating substrate. The oxides used in thick films mainly classified into two groups: (i) metallic oxides in which the resistivity usually obeys a power law dependence on temperature, $\rho \propto T^n$, where $n > 0$; and (ii) semiconducting oxides, for which the resistivity usually follows an exponential law, $\rho \propto \exp(E/KT)$, where E is activation energy; K is Boltzmann constant and T is absolute temperature.

According to the Tatamangalam [40], the resistance of oxide thick film can be decreased normally due to increase in temperature of the thick film, which causes the electrons to acquire enough energy and cross the barrier at grain boundaries. Due to this, the effective resistance of thick film drops down to steady level at high temperatures, i.e. the decrease in resistance with increase in temperature of oxide thick films can be attributed to (i) decrease in potential barrier at grain boundaries, since at higher temperatures, the oxygen adsorbents are desorbed from the surface of the films [37]; (ii) at higher temperature the carrier concentration increases due to intrinsic thermal excitation, and Debye length decreases and (iii) an electron emission process, which always improves with increase in temperature. The electrical resistivity is found to be varying exponentially with the temperatures, suggesting that the conduction mechanism is thermally activated. The decrease in resistance with increase in temperature is due to increasing drift mobility of the charge carriers or due to the lattice vibrations associated with increasing temperature, where the atoms occasionally come close enough for the transfer of charge carriers and conduction is induced by lattice vibrations [41].

The saturation region is a region with very low activation energy. This region may indicate some saturation levels due to surface unevenness. In order to see that the fall in resistance is due to activation process, the corresponding Arrhenius plots are plotted.

The high resistance for Oxide thick films may be due to the (i) deficiency of oxygen ions. When exposed to atmospheric oxygen, the oxygen is adsorbed at the surface of the film. The free electrons in the grains in contact with this adsorbed oxygen molecules are trapped due to their high electron affinity. The resultant negative charge built-up at the boundaries causes a high potential barrier at the boundary. This hampers the free movement of the electrons across the boundary, which is reflected as a corresponding increase in the effective resistance of the ceramic (oxide film) material. (ii) Random distribution of grains, with more porosity in the film and (iii) due to poor crystallinity.

Yamazoe et al. have suggested that oxygen adsorbs onto the surface of SnO_2 and ionizes to O^- or O^{2-} depending on the temperature by trapping electrons from the lattice [42]. Similar mechanism can be adopted in the case of WO_3 . The resistance decreases with increase in firing temperature is related to the low concentration of the adsorbed oxygen or the trapped electrons on the surface because the ratio of the surface area to bulk or the adsorbed oxygen concentration decreases with the increase in grain size. The firing temperature can change surface characteristics including grain size, surface area, and crystallinity [43].

Fig. 5(b) shows the $\log R_s$ variation with reciprocal of temperature of WO_3 thick films fired at 600, 700 and 800 °C temperatures. The curve shows two regions of variations in resistance with temperature having different activation energies. The two distinct regions of temperature viz low temperature region (303 to 423 °K) and high temperature region (423°K to 723 °K). The activation energy in the lower temperature region is always less than the energy in the higher temperature region because material passes from one conduction mechanism to another. The earlier reported value of activation energy is 0.82 eV [44]. In low temperature region, the increase in conductivity is due to the mobility of charge carriers which is dependent on the defect/dislocation concentration. So, the conduction mechanism is usually called the region of low temperature conduction. In this region activation energy decreases, because a small thermal energy is quite sufficient for the activation of the charge carriers to take part in conduction process. In other words the vacancies/ defects weakly attached in lattice can easily migrate (extrinsic migration). Hence increase in the conductivity in the lower temperature region can be attributed to the increase in charge mobility.

Fig. 6(a) shows the variation of resistivity with firing temperature of WO_3 thick films. It is seen that the resistivity decreases with increase in firing temperature of the films may be attributed to an increase the grain size with the firing temperature supported by the results from XRD and SEM analysis. Temperature coefficient of resistance (TCR) of WO_3 thick films is negative for all samples, indicating semiconducting behaviour. The variation of TCR with firing temperature of WO_3 Thick films is shown **Fig. 6(b)**. TCR is maximum at 800°C firing temperature can be attributed to increase in the degree of crystallinity and grain size with firing temperature.

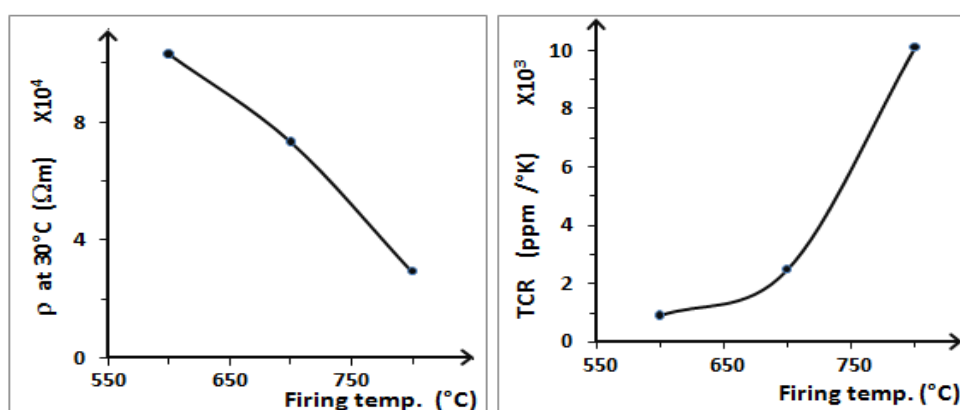


Fig. 6 Plot of (a) Resistivity and (b) TCR versus firing Temperature of WO₃ thick films

Activation energy for low temperature (LT) and high temperature (HT) regions of WO₃ thick films was calculated from log R versus 1/T curve by using the relation $R=R_0e^{-\Delta E/KT}$. Fig.7 illustrates variation of Activation energy with Firing Temperature of WO₃ thick films. The variation of activation energy values with increase of firing temperature are shown in fig. 7.

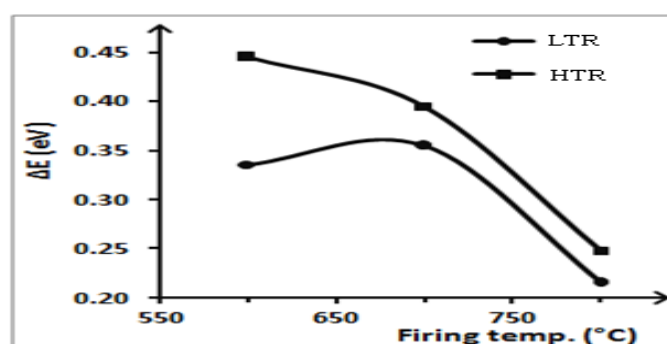
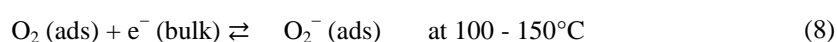


Fig.7 Activation energy versus Firing Temperature of WO₃ thick film resistors

4.2. Gas sensing characterization

This section deals with the study of gas sensing properties of WO₃ Semiconductor metal oxide thick film resistor sensors fired at optimized temperature of 600°C. Semiconductor metal oxide-based gas sensors are extensively used for detection of several toxic, inflammable and odourless gases [45-50]. As the gas sensors are resistive type in the form of thick films, the electrical characterization is related to the resistance variation with operating temperatures in different gaseous medium at ppm level of gas (H₂S, NO₂, C₂H₅OH, NH₃, O₂ and LPG) at normal atmospheric conditions. The Metal Oxide gas Sensor follows some basic mechanism during gas sensing like surface reaction with adsorbed gases, ion exchange and direct gas adsorption. In the presence of test gases, the electrical conductivity of porous semiconductor thick film sensor changes due to two main reactions occurring on the surface [51-52]. These reactions are the adsorption of atmospheric oxygen on the surface and the direct reaction of lattice oxygen or interstitial oxygen with test gases. In the first reaction, atmospheric oxygen molecules are physisorbed on the surface sites, which while moving from site to site, get ionized by taking an electron from the conduction band and are thus ionosorbed on the surface as O_{ads} [53]. This causes decrease in conductance of sensor material. In short, Oxygen molecules from air adsorbed on surface of metal oxide removing electrons from conduction band of sensing metal oxide and occur on surface in form of O⁻, O²⁻ and O₂⁻ depending on temperature, creating a thin layer of depletion region at the surfaces of WO₃ grains [54-56]. The resulting equations are,

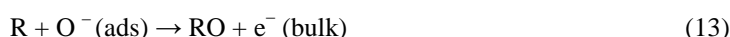




In WO_3 films, electrons are also extracted from the interstitial tungsten atoms W, which act as an electron donor [57]. The interstitial tungsten atoms in such cases are ionized via the following reversible reaction,



In the second step the reducing gas molecule present in air ambient reacts with the chemisorbed oxygen, thereby releasing an electron back to the conduction band and increasing the conductance of the semiconductor,



At higher temperature RO desorbs.

Response to a gas is related generally to the number of oxygen ions adsorbed on the surface of film. If film surface chemistry is favorable for adsorption, response and selectivity would be enhanced. In case of pure WO_3 , oxygen adsorption seems to be poor which may result in poor response. In addition to this, WO_3 requires relatively larger operating temperature to adsorb the oxygen ions and therefore it would have responded at higher operating temperature [58].

4.2.1. Gas sensing response of NO_2 gas

Fig. 8 shows the pure WO_3 thick film gas sensor response for different gases (H_2S , NO_2 , $\text{C}_2\text{H}_5\text{OH}$, NH_3 , O_2 and LPG) to 500ppm. WO_3 Gas sensing response was measured in air at a temperature range 100 to 450°C . The temperature scan rate used for the study gas sensing response is nearly constant and slow ($\approx 10^\circ\text{C}/\text{min}$). Sensors were not sensitive to test gas at room temperature. In general, it is known that the metal oxide sensor is affected by the working temperature. The higher temperature enhances surface reaction of the sensor and gives higher sensitivity in a temperature range. Amount of chemisorbed oxygen on surface and the surface species available for adsorption highly influences the change in conductivity. The fig. 8 presents the effect of temperature on WO_3 thick film resistive gas sensors prepared by using standard screen printing method and fired at 600°C . The pure WO_3 thick films show considerable response to NO_2 gas. The resistance of films increases when exposed to the NO_2 gas. The maximum sensitivity observed for NO_2 is 24.31 at 290°C which is higher than other studied gases.

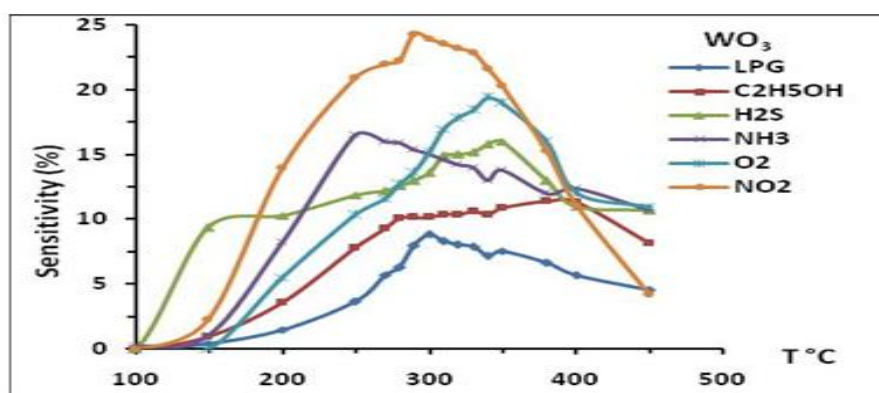
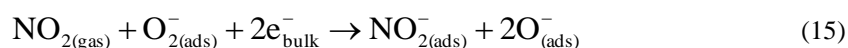


Fig. 8: Plot of sensitivity Vs temperature of WO_3 thick films fired at 600°C for different gases at 500 ppm

Nitrogen dioxide is a strong oxidizing agent and has strong electrophilic property [59], which makes this molecule to be quickly adsorbed on the metal oxide surface. NO_2 can react with metal oxide surface both in the presence and absence of oxygen. The oxidation of NO_2 leads to the reduction of conduction electrons in the conduction band and hence the detection of NO_2 is achieved.





Thus the cyclic reaction continues. These series of reactions resulted in the concentration of electron on the surface of the material to further decrease, which led to the decrease in conductivity of the material.

Also adsorption of oxygen from the NO₂ molecule on to the vacant site leads to decrease in conductance of the n-type metal oxide [60].



Fig. 9 illustrates the gas sensing mechanism. NO₂ is oxidizing gas. Changes in the conductivity are caused by electron transfer between adsorbed molecules and the semiconductor surface. The electrical conduction takes place via individual WO₃ grains. NO₂ gets chemisorbed at the surface of WO₃ grains. Hereby they trap electrons at the surface. WO₃ is an n-type semiconductor. The electrons are taken from ionized donors through conduction band and the density of majority charge carriers at the gas–solid interface is reduced. This leads to the formation of a potential barrier for electrons with increasing of the oxygen ions density on the surface the further oxygen adsorption is inhibited. Thus at the junctions between WO₃ grains, the depletion layer and potential barrier leads to the increasing of the electrical resistivity value. This value is strongly dependent on the concentration of adsorbed oxygen ions of the surface. Introducing the n-WO₃ films in an NO₂ ambient will change the concentration of these ions and increase the resistance.

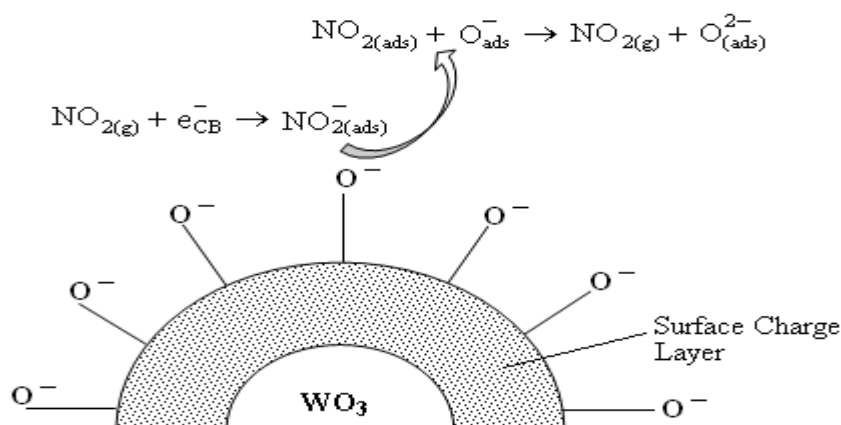


Fig. 9 Gas sensing mechanism

For NO₂ gas, the response was observed to increase with operating temperature (**Fig 8**) up to 290°C. After 290 °C temperature, the surface would be unable to oxidize the gas so intensively and the NO₂ may burn before reaching the surface of the film at higher temperature. Thus, the gas sensitivity decreases with increasing temperature [61]. The higher sensitivity may be attributed to the optimum number of misfits on the surface, porosity, larger surface area and the larger rate of oxidation of NO₂ at 290 °C for thick film. The maximum response of WO₃ thick film to NO₂ gas was found to be 24.31 at 290°C.

4.2.2. Selectivity of NO₂ against other gases

Selectivity or specificity is defined as the ability of a sensor response to a certain (target) gas in the presence of other gases. Percent selectivity of one gas over others is defined as the ratio of the maximum response of other gas to the maximum response of target gas (at optimum temperature of target gas) [62, 63]. The selectivity of the films for the particular gas with respect to other was determined by the relation,

$$\% \text{ Selectivity (S)} = \left(\frac{\text{Sensitivity of interfering gas}}{\text{Sensitivity towards desired gas}} \right) \times 100 \quad (18)$$

Fig. 10 shows histogram for the selectivity of other gases against NO_2 at 290°C . The selectivity of NO_2 is considered as 100%. It is observed from histogram that the WO_3 thick films are sensitive to NO_2 gas and it has relatively good selectivity against other gases. This is the main feature of pure WO_3 thick film sensor. It is also observed that, the WO_3 thick films also responds to other gases, though less. The efforts therefore must be taken to enhance the sensitivity and selectivity of the WO_3 thick film sensor to the other gases at different operating conditions.

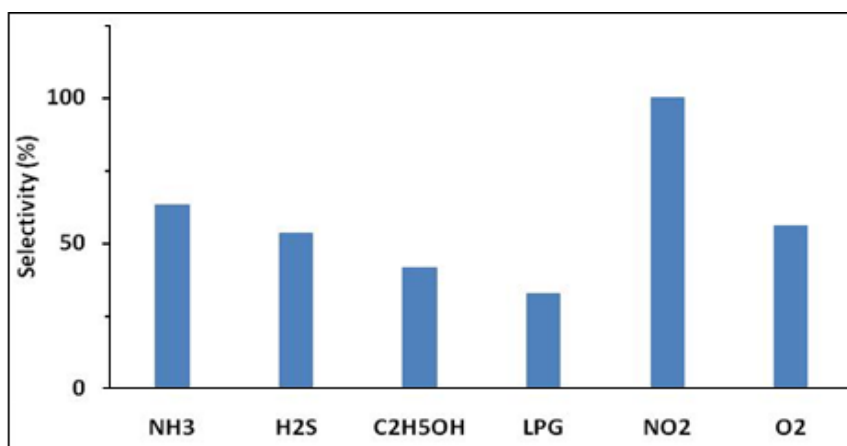


Fig. 10 Selectivity of WO_3 thick film sensor for different gases against NO_2 gas at 290°C

4.2.3. Variation of Sensitivity with gas concentration (ppm)

Fig. 11 shows variation of sensitivity of WO_3 thick film sensor for NO_2 for different gas concentrations in ppm level at the optimum temperature 290°C . The most important specifications of any sensor is obviously its calibration curve to find the concentration dependence of sensitivity, a series of observations are carried out for the best of WO_3 thick film resistive sensor fired at 600°C . For this study, two samples are temperatures scan, each at least two times to get the optimal temperature at each concentration (from 100ppm to 1000ppm). The change in optimal temperature with concentration is negligible. It is seen that the rate of increase in response is relatively larger up to 600 ppm and then saturates. So we can infer that the active region of the WO_3 film resistor would be between 100 to 600 ppm.

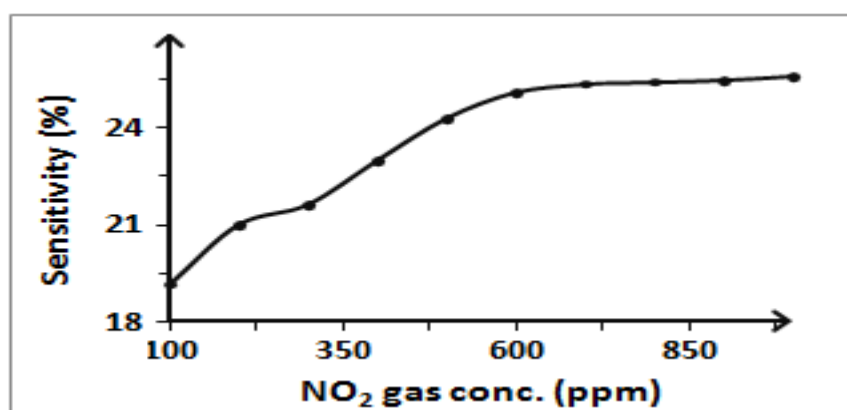


Fig. 11 Sensitivity of WO_3 thick film as a function of NO_2 gas concentration at 290°C .

4.2.3. Response and recovery time of the sensor

The response/recovery time is an important parameter used for characterizing sensors. It is defined as the time required to reach 90% of the final change in voltage or resistance, when the gas is turned ON or OFF, respectively. The response and recovery times of WO_3 film samples are represented in **Fig. 12**. The response was quick (~ 16 s) to 500 ppm of NO_2 while the recovery was fast (~ 42 s). The quick response may be due to faster oxidation of gas. Its high volatility explains its quick response and fast recovery to its initial chemical status.

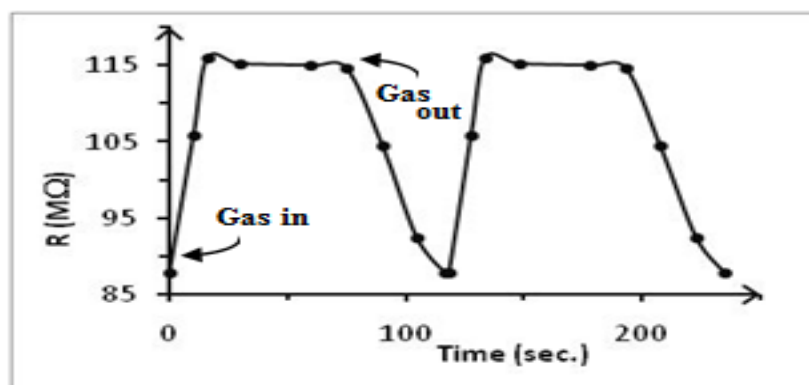


Fig. 12 Response and recovery times of WO₃ film samples to NO₂ gas

V. Conclusions

This paper presents the successful preparation of WO₃ thick film shows good adhesion to alumina substrate employing a simple, inexpensive screen printing method. and electrical characterization of WO₃ films. The thick films were characterized by using XRD and SEM coupled with EDAX. WO₃ thick films show polycrystalline nature. The electrical parameters viz. resistivity, TCR and activation energies were evaluated by usual methods. WO₃ thick films exhibited good sensing performance to NO₂ gas with maximum sensitivity, 24.31 at 290 °C, with fast response and recovery time. Further, it was shown that the screen printed WO₃ thick films can be reliably used to monitor the concentration of gas over the wide range. The response and recovery characteristics of WO₃ thick films are almost reproducible and quick. Thus, this study demonstrates the possibility of utilizing WO₃ thick films as a sensor element for the detection of NO₂ gas.

Acknowledgement

The author is grateful to Management authorities of M.G. Vidyamandir, Panchavati, Nasik for providing laboratory facilities for doing the work. Author sincerely thanks U.G.C. for awarding the teacher fellowship under XIIth under FDP programme.

References

- [1] M. A. Butler J. Appl. Phys. **48** (1977) 1914-1920.
- [2] Y. M. Hunge, M. A. Mahadik, S. S. Kumbhar, V. S. Mohite et al. Ceram. Int., **2016**, 42, 789-798.
- [3] M. A. Ouis, H. A. El-Batal, M. A. Azooz and M. A. Abdelghany. Indian Journal of Pure & Applied Physics, **51-1** (2013) 11-17.
- [4] K. J. Choi, and H. W. Jang, Sensors **10** (2010) 4083-4099.
- [5] W. L. Kwong, A. Nakaruk, P. Koshy, C. C. Sorrell, Thin Solid Films, **2013**, 544, 191-196.
- [6] Y. Shen, L. Pan, Z. Ren, Y. Yang, Y. Xiao, Z. Li, J. Alloys Compd., **2016**, 657, 450-456.
- [7] L. E. Jose, A. R. Manuel, M. Jose, H. Abel, Thin Solid Films, **2016**, 606, 148-154.
- [8] K. Khojier, H. Savaloni, N. Habashi, M. H. Sadi, Mater. Sci. Semicond. Process. **2016**, 41, 177-183.
- [9] A. Karuppasamy, Appl. Surf. Sci., **2013**, 282, 77-83.
- [10] A. I. Gavriluk, Appl. Surf. Sci., **2016**, 377, 56-65.
- [11] J. Xue; Y. Zhu, M. Jiang, J. Su, Y. Liu, Mater. Lett., **2015**, 149, 127-129.
- [12] P. Woodward P. and A. Sleight A. Journal of Solid State Chemistry, **131** (1997) 9-17.
- [13] T. Vogt, P. M. Woodward and B. A. Hunter. Journal of Solid State Chemistry **144** (1) (1999) 209-215.
- [14] Salje E. Acta Crystallographica B **33** (2) (1977) 574-577.
- [15] W. L. Kehl, R. G. Hay, D. Wahl, Journal of Applied Physics **23** (2) (1952) 212.
- [16] Diehl R, Brandt Gand Saije E: The crystal structure of triclinic WO₃, Acta Crystallographica B **34** (4) (1978) 1105-1111.
- [17] B. Gerand, G. Nowogrocki, J. Guenot, and M. Figlarz. Journal of Solid State Chemistry **29** (3) (1979) 429-434.
- [18] S. K. Gullapalli, R. S. Vemuri, F. S. Manciu, J. L. Enriquez, C.V. Ramana, J. Vacuum Sci. Technol., A, **2010**, 28, 824-828.
- [19] A. I. Nishchay, V. Marco, S. Andreas, B. George, ACS Appl. Mater. Interfaces, **2016**, 8, 3933-3939.
- [20] C. Wongchoosuk, A. Wisitsoraat, D. Phokharatkul, A. Tuantranont, and T. Kerdcharoen, Multi-walled carbon nanotube-doped tungsten oxide thin films for hydrogen gas sensing, Sensors **10**, 7705-7715, (2010).
- [21] R. Y. Borse and A. S. Garde, Indian J Physics, **82** (10) (2008) 1319-1328.
- [22] Ratan Y. BORSE, Vaishali. T. SALUNKE and Jalinder AMBEKAR, Effect of Firing Temperature on the Micro Structural Parameters of Synthesized Zinc Oxide Thick Film Resistors Deposited by Screen Printing Method, Sensors & Transducers Journal, Vol. 144, Issue 9, September 2012, pp. 45-61 ISSN 1726-5479
- [23] S. G. Ansari, P. Boroojerdian, S. K. Kulkarni, S. R. Sainkar et al., Effect of Thickness on H₂ gas sensitivity of SnO₂ nano particles based thick film resistors, Journal of Materials Science: Materials in Electronics, 7, 1996, pp. 267-270.
- [24] Maria Prudenziati; Bruno Morten, Thick film Sensors. An Overview, Sensors and Actuators, 10, 1986, pp. 65-82.
- [25] Harper C. A, Handbook of Thick film hybrid Microelectronics, (McGraw Hill Book Co., New York, 1974).

- [26] Kiran Jain, R. B Pant, S. T. Lakshmi kumar, Effect of Ni doping on thick film SnO₂ gas Sensor, *Sensors and Actuators, B*, 113, 2006, pp. 823-829.
- [27] Ramkumar K., *Thick Film Deposition and Processing*, short term course on thin and thick Film hybrid Microelectronics, (Bangalore, 1986).
- [28] A. T. Nimal, Vijay Kumar and A. K. Gupta, Superconducting transition edge bolometer based on single phase BPSCCO2223 thick film, *Indian Journal of pure and applied physics*, Vol. 42, 2004, pp. 275-278.
- [29] L. A. Patil, Wani P. A., Sainkar S. R., Mitra A., Pathak G. J. and Amalnerakar D. P., Studies on “fritted” thick films of photoconducting CdS, *Mater. Chem. Phys*, 55, 1998, p. 79.
- [30] B. D. Cullity, *Elements of X-ray diffraction*, (Addison-Wesley Publishing Co., 1956).
- [31] M.N. Romyantseva, A.M. Gaskov, N. Rosman, T. Pagnier, J.R. Morante, *Chem. Mater.* 17 (2005) 893–901.
- [32] J. Zhang, L. Gao, *Mater. Res. Bull.* 39 (2004) 2249–2255.
- [33] William Frank Macculm (editor-in chief), *Powder diffraction Files*, JCDP, (International center for diffraction Data, Pennsylvania, USA).
- [34] G. Sarala devi, S. Manoramma and V. J. Rao, Gas sensitivity of SnO₂/CuO Hetrocontacts, *J. Electrochemical Soc.*, 142, 8, 1995, pp. 2574-2577.
- [35] Duk-Dong Lee, *Thick-film Hydrocarbon gas Sensors*, *Sensors and Actuators, B*, 1990, pp. 231-235.
- [36] G. H. Jain and L. A. Patil, Gas Sensing properties of CuO and Cr activated BST thick films, *Bulletin of material science*, Vol. 29, No. 4, 2006, pp. 403-411.
- [37] H. Windichmann and P. Mark. *J. Electrochem. Soc.* 126 (1979) 627-633.
- [38] N. Niffontoff, *Comp. Rend*, 236 (1953) 1538; 237 (1953) 24.
- [39] K. M. Anisur Rahman, Susan C. Schneider, and Martin A. Seitz. *J. Am. Ceram. Soc.* 80 (5) (1997) 1198-1202.
- [40] R. P. Tatamangalam, *Industrial Instrumentation Principles and Design*, (Springer Press, 13 Dec. 1999).
- [41] K. Ramkumar, *Characterization of Films*, Short-Term Course on Thick and Thin Film Hybrid Microelectronics, (Bangalore, P12.11 (1986)).
- [42] N. Yamazoe, K. Ihokura, J. Watson (Eds.), *The Stannic Oxide Gas Sensor: Principles and Applications*, (CRC Press, Boca Raton, 1994, p. 66).
- [43] Hyun-Wook Ryu, Bo-Seok Park, Sheikh A. Akbar, Woo-Sun Lee et al. *Sensors and Actuators B* 96 (2003) 717–722.
- [44] Barsan N, Gopel W: Fundamental and practical aspect in design of nanoscale SnO₂ gas sensor: a status report. *Journal of Analytical Chemistry* 365(4) (1999)287-304.
- [45] C. Zhang, M. Debliquy, A. Boudiba, H. Liao, C. Coddet. *Sensors and Actuators B* 144 (2010) 280–288.
- [46] A. Boudiba, C. Zhang, C. Navio, C. Bittencourt et al. *Procedia Engi.* 5 (2010) 180–183.
- [47] C. Zhang, A. Boudiba, C. Navio, M.G. Olivier et al. *Sensors and Actuators B* 161 (2012) 914–922.
- [48] K. Paipitak, C. Kahattha, W. Techitdheera, S. Porntheeraphat. *Energy Procedia* 9 (2011) 446–451.
- [49] W. Li, J. Li, X. Wang, S. Luo, J. Xiao. *Electrochimica Acta* 56 (2010) 620–625.
- [50] K. J. Choi, and H. W. Jang, *Sensors* 10 (2010) 4083–4099.
- [51] J. Dayan, S. R. Sainkar, R. N. Karekar, R. C. Aiyer, *Thin Solid Films* 325 (1998) 254–258.
- [52] H. Windichmann, P. Mark. *J. Electrochem. Soc.* 126 (1979) 627-633.
- [53] J. Marc, S Madau, R. Morrison, *Chemical sensing with Solid State Devices*, Academic Press, New York, 1989
- [54] Vibha Srivastava, Kiran Jain. *Sensors and Transducers Journal* 117 (6) (2010) 120-128.
- [55] A. Al. Mohammad. *Acta Physica Poloncia* 116 (2009) 241-244.
- [56] N. B. Sonawane, D. R. Patil, L. A. Patil. *Sensors and Transducers J.* 93 (6) (2008) 82-91.
- [57] M. Takata, D. Tsubone, H. Yanagida, *J. Am. Ceram. Soc.* 59 (1-2) (1976) 4- 8.
- [58] L. A. Patil, I. G. Pathan, *Sensors & Transducers Journal* 108 (9) (2009) 180-188.
- [59] S. L. Bai, J. W. Hu, D. Q. Li, R. X. Luo et al. *IEEE Sens. J.* 12 (2012) 1122-1126.
- [60] S. Kannan, H. Steinebach, L. Rieth, F. Solzbacher. *Sens. Actuat. B* 148 (2010) 126.
- [61] G. H. Jain, L. A. Patil. *Bulletin of Material Science* 29 (4) (2004) 403-411.
- [62] G.H. Jain, L.A. Patil, V.B. Gaikwad, *Sensors and Actuators B* 122 (2007) 605–612
- [63] D.R. Patil, L.A. Patil. *Sensors and Actuators B* 123 (2007) 546–553